This is a previous version of the article published in Colloids and Surfaces A: Physicochemical and Engineering Aspects. 2022, 652: 129882
https://doi.org/10.1016/j.colsurfa.2022.129882

Activated carbon from polyurethane residues as molecular sieves for kinetic adsorption/separation of CO_2/CH_4

Orlando F. Cruz Jr.[1], Ignacio Campello Gómez[2], Manuel Martinez Escandell[2], Carlos R. Rambo[3*], Joaquín Silvestre-Albero[2]

[1] Laboratory of Microscopy and Nanotechnology, National Institute of Amazonian Research
69067-375, Manaus, Brazil
[2]Departamento de Química Inorgánica, Universidad de Alicante,
E-03080 Alicante, Spain
[3] Department of Electrical and Electronic Engineering, Federal University of Santa Catarina,
88040-900 Florianópolis, Brazil

Abstract

Activated carbon-based molecular sieves were synthetized, characterized and their kinetics of adsorption were evaluated to be used in separation processes of CO_2/CH_4 mixtures. Polyurethane (PU) foams were used as carbon precursor and the PU-derived carbons were physical activated with CO_2. All the samples present a preferential adsorption of CO_2 over methane in kinetic adsorption experiments. Samples activated at 800 ºC during 6 h exhibited the higher selectivity due to the absence of methane adsorption at lower resident times, which makes those samples very interesting for industrial processes of natural gas purification. Kinetic studies were performed to explain the kinetic profiles obtained, confirming that in the samples with smallest pore size, intraparticle diffusion was the limiting step, evidencing that certain oxygen groups favour CO_2 adsorption, whereas adsorption was the limiting step in the samples with wider pores.

Keywords: Carbon molecular sieves; CO_2 adsorption; natural gas separation; adsorption kinetics.

*Correspondence should be addressed to:
Carlos R. Rambo: carlos.rambo@ufsc.br (ORCID: 0000-0001-5192-7277)

1. Introduction

Emissions of CO_2 and global warming are very concerning issues due to the negative environmental impact. CO_2 emissions have been widely proved as responsible for the global warming [1], and these emission are far for being reduced. For these reasons, there is a huge interest in technologies that avoid the use of fossil fuels, such as their substitution with methane. Methane represents a cleaner alternative for fossil fuels, and there is a rise in the technology investment on this field. One of the major inherent impurities present in natural gas current flows is CO_2. This CO_2 impurity has to be reduced in order to purify methane flows, since CO_2 reduces the caloric input. Moreover, it represents the most difficult and most expensive step of methane purification [2], and hence, there is a lot of interest in the development of materials and processes capable to purify methane.

There are several technologies that allow the purification of CO_2/CH_4 mixtures; some of them are based on the higher solubility of CO_2 in certain solvents such as water or organic solvents [3,4], but they present important disadvantages such as corrosion and the complexity of the systems. Another approach is the amines adsorption, which also has drawbacks like its highly energy demand during the process and the corrosion caused by the amines used [5,6]. It is also possible to use membranes for this purpose, where the larger retention of methane than CO_2 allows their separation. This process, however, requires the use of high pressure and CO_2-rich flows, whereas the membranes exhibit a short lifetime [4]. Finally, there are some cryogenic technologies to carry out the separation, but they have significant energetic needs in order to be efficiently performed [7].

One of the main approaches to this issue is the development of molecular sieves for adsorption process separation. A molecular sieve is a material which is able to discriminate the adsorption of one molecule due to its size. In this case, since CO_2 kinetic diameter is lower than methane (3.3 *vs* 3.7 Å), materials with a range of pore size lower than 3.7 Å are

needed. This process will allow a complete separation of those gases, and hence, the production of a methane flow with high purity using a low cost process such as pressure swing adsorption (PSA) [8,9]. For separation processes, physically activated carbons (AC's) are an interesting solution, especially when they are sustainably produced from waste residues or biomass [10-13]. Li et. al [14], for instance, reported biomass-derived (grapefruit peel and banana peel) AC's for separation of $CO_2/NH_4/N_2$ mixtures. Activated carbons are suitable for swing adsorption processes, PSA, which due to their good performance and simple mechanism, are a topic of great interest for the industry. This technology consists on the performance of sorption and desorption cycles of a current flow applying certain pressure, where the easiness of desorption cycles of solid adsorbents makes them very suitable candidates for the process.

Polyurethane, PU, is the fifth most used polymer in Europe [15]. PU foams are present in many applications for building industry, vehicular and aeronautics applications or different industrial machinery due to their characteristics and good performance as low density insulators. One of the major problems of these materials is their recyclability, since PU is a thermostable polymer and hence, does not undergo a fluid phase when heated. Therefore, their recyclability consists on the crushing of the material in smaller pieces in order to fulfil different structures. For all these reasons, PU foams are an excellent source for the synthesis of very cheap and available carbon materials.

This work reports, therefore, the use of PU residues as carbon source for producing activated carbons as molecular sieves for CO_2/CH_4 separation processes.

2. Experimental

Synthesis

The synthesis of the AC's was carried out in horizontal tubular furnaces. First, a piece of commercially available PU foam was ground to sizes between 1-2 mm and, afterwards, pyrolysed in nitrogen atmosphere at 400 ºC using a flow of 100 mL/min during 2 hours with a heating rate of 10 ºC/min. The activation was performed at different temperatures ranging from 800 °C to 950 °C for 6, 7 or 12 h using a 80 mL/min flow of CO_2 and a heating rate of 10 ºC/min. Samples were named according to their activation temperature and time of activation as follows: PU (Activation temperature in ºC) (Activation time in hours). Hence, a sample activated at 900 ºC for 6 hours is named as: PU 900 6H.

In order to obtain PU precursors with more similarities to real residues, another piece of PU foam was exposed to an oxidant atmosphere at 70 ºC for 3 months, which resulted in a red coloured material, typical of this kind of PU residues. The activated carbon materials obtained were named as PUox and were pyrolysed and activated following the same procedure used for the other PU samples.

Characterization

Thermogravimetric analyses (TGA/SDTA 851e/SF/1100, Mettler Toledo) under inert atmosphere were carried out to study the behavior of pure PU foam waste and the pyrolysed PU carbons. Textural properties of the activated carbons were investigated using nitrogen and CO_2 isotherms as well as the calculations related to this technique. Nitrogen isotherms at -196ºC and CO_2 at 0 and 25ºC isotherms were performed in an Autosorb-6 gas sorption system (Quantachrome Instruments). BET surface area and micropore volume, V_0, was determined from the nitrogen adsorption data after application of the BET and the Dubinin-Radushkevich (DR) equations, respectively [16]. Apparent BET surface area was obtained in the P/P_0 range from 0.02 to 0.12 for narrow sized microporous samples. The total pore volume (V_t) was measured at $P/P_0 \approx 0.95$. The volume of narrow micropores (V_{CO2}) was

calculated from CO_2 isotherm at 0 ºC by applying the DR equation. Pore size distribution was calculated by the application of the Quenched-Solid Density Functional Theory (slit pore, QSDFT equilibrium model) to the nitrogen adsorption isotherm data for pores with size below 1 nm. External surface area (S_{ext}) was calculated using de Boer's t-plot (statistical thickness) method, with statistic thickness t ranging from 2.0 to 5.0 Å. Micropore surface area (S_{mic}) was then estimated from the relation $S_{mic} = S_{bet}-S_{ext}$. X-ray photoelectron spectroscopy (XPS) analysis was applied to evaluate surface nitrogen and oxygen groups. A K-Alpha spectrometer from Thermo-Scientific was used. The analysis chamber was held under vacuum below 5×10^{-9} mbar during analysis.

Kinetic measurements

The kinetic analysis was performed in a glass system using an oil vacuum pump able to reach a vacuum of 10^{-4} mmHg, measured with a Pirani detector. Prior to the experiments, 4 h of vacuum at 150 ºC was applied to degas the samples and the system. Then, 700 mmHg of CO_2 or methane within a known volume were loaded to the sample, and the decrease in pressure was related to the amount of gas adsorbed. The initial volume of the system with the sample was measured by the same procedure but using helium as inert gas. The instrument was coupled to a system able to record up to 2 points/measurements per second.

3. Results and discussion

In order to asset and compare thermal stability of PU and PUox samples, TG experiments under flowing N_2 atmosphere were performed. The decomposition profiles shown in **Figure 1**, indicate that PUox starts the weight loss at lower temperature than PU, with almost 100 ºC of difference. Moreover, both samples reached the same weight loss at 1000 ºC and, therefore, one can state that no important structural changes took place during aging of PUox.

This feature may indicate that the oxygen functionalities generated during oxidation helps to initiate the decomposition reactions and, thus, the release of volatiles initiate at lower temperatures.

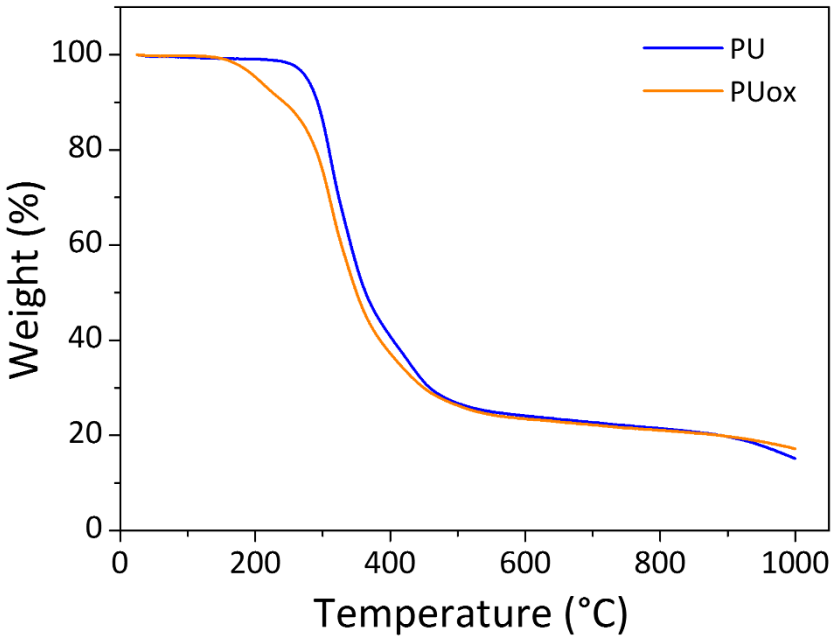

Figure 1. TG profiles of PU and PUox samples performed under nitrogen atmosphere.

Figure 2 shows N_2 isotherms at -196 °C (Fig. 2a), CO_2 at 0 °C (Fig. 2b) and at 25 °C (Fig. 2c) and pore size distribution (Fig. 2d) resulted from applying the DFT method to the adsorption isotherm data. **Table 1** summarizes the data obtained from those isotherms. All the isotherms are microporous type I isotherms, which means that they all present narrow porosity. The differences in the activation of PUox 800 6H and PU samples could be explained since according to the TG measurements PUox samples is thermally less stable than PU sample, and hence, more susceptible to activation.

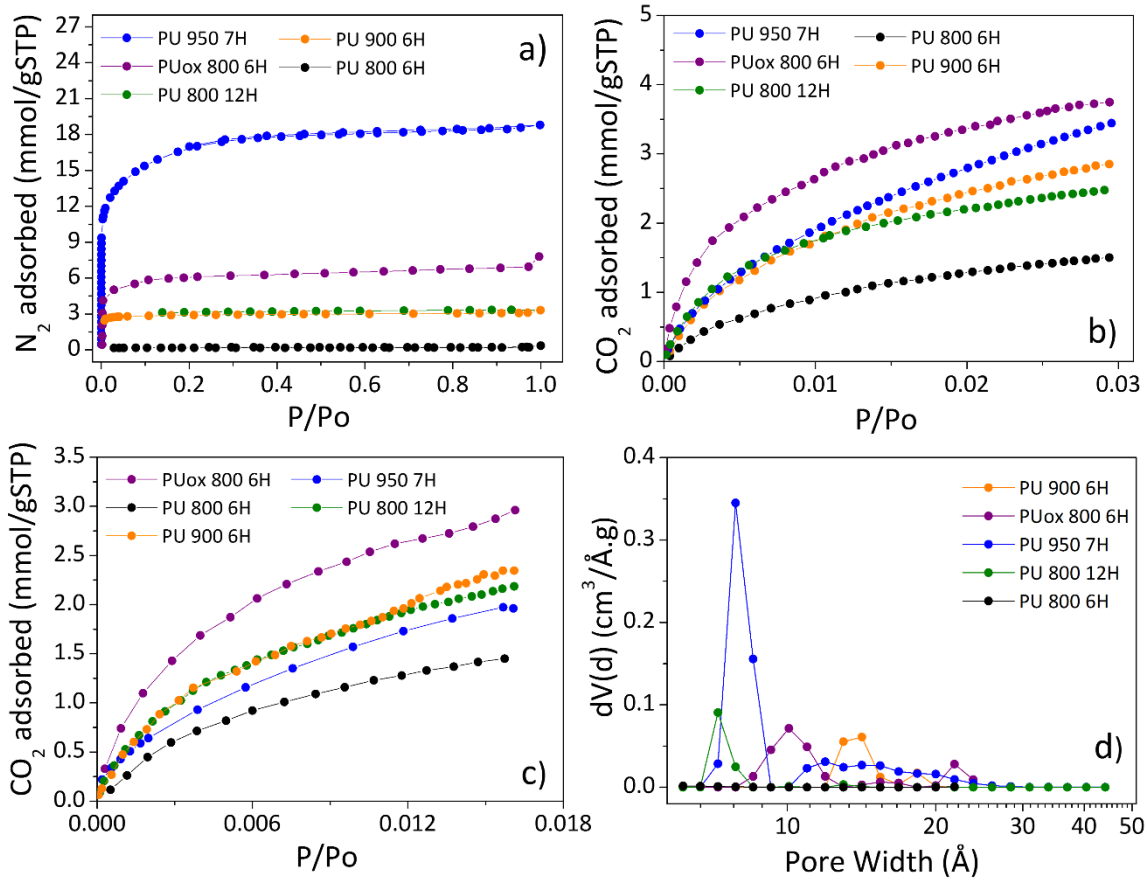

Figure 2. (a) Nitrogen isotherms at -196 ºC; (b) CO_2 isotherms at 0 ºC; (c) CO_2 isotherms at 25 ºC and (d) Pore size distribution obtained by DFT method.

It can be observed how the activation conditions influence the development of porosity. Activation temperature influences N_2 and CO_2 adsorption to a larger extent than activation time. Hence, N_2 and CO_2 adsorption increase with the activation temperature, especially when reaction takes place at 900ºC. No N_2 adsorption at -196 ºC occurred in the sample activated at 800 during 6 h. Therefore, this sample is a good candidate to act as a molecular sieve, with no adsorption of methane, since the kinetic diameter of methane is higher than that of nitrogen. PUox 800 6H sample exhibits the highest CO_2 adsorption despite its lower BET surface area (S_{bet}) and microporous surface (S_{mic}) than the sample activated at 950 ºC, which indicates the presence of a microporous structure and narrow porosity. Moreover, the ratio S_{mic}/S_{bet} is similar (around 0.47) for both PUox 800 6H and PU

950 7H samples. It must be noticed that the kinetic diameter of nitrogen and methane are 3.6 and 3.8 Å, respectively, and therefore, it is possible to obtain samples with such a porosity where nitrogen could be adsorbed but not methane, although unusual.

Table 1. Textural properties of the synthetized samples.

Precursor	Time (h)	Temp. (ºC)	S_{bet} (m^2/g)	S_{mic} (m^2/g)	V_t (cm^3/g)	V_0 (cm^3/g)	V_{co2} (cm^3/g)	*N_{co2} (mmol/g)	Burn off (%)
PU	6	800	<1	---	<1	<1	0.14	1.5	69
PUox	6	800	490	228	0.24	0.22	0.29	3.7	73
PU	12	800	<1	---	<1	<1	0.27	2.6	74
PU	6	900	300	117	0.15	0.14	0.29	2.9	88
PU	7	950	1330	643	0.64	0.51	0.25	3.4	92

*273 K, 1 bar S_{bet}: ''Apparent'' surface area calculated using the BET method; S_{mic}: surface microporosity; Vt: Total pore volume obtained from the amount of N_2 adsorbed at p/p0 ~ 0.95; V0: Micropore volume calculated by applying the DR equation to the N_2 adsorption data at -196ºC; V_{co2}: Volume of narrow micropores calculated by applying the DR equation to the CO_2 adsorption data.

All the samples except PU 950 7H present a higher CO_2 micropore volume, V_{CO2}, than the total pore volume, V_t, obtained from nitrogen isotherms; hence, indicating the presence of very small microporosity, accessible for CO_2 but not for N_2. This suggests that CO_2 will be more preferentially adsorbed than methane, since the kinetic diameter of methane is larger than that of nitrogen. The CO_2 adsorption values are very similar when comparing the isotherms at 25 °C and 0 ºC (Fig. 2b and c). Additionally, the micropore volume obtained using CO_2 isotherms, V_{CO2}, is higher than the nitrogen micropore volume, V_0, in all the cases, except for the activation at 950 ºC, which is an indication of the narrow microporosity formed, where pores seem to be smaller than the kinetic diameter of N_2.

The pore size distribution of the AC's (Fig. 2d) reveals different pore size ranges for all samples. Adsorption in the sample activated at 800 °C for 6 hours is low, as indicated by pores with sizes lower than 6 Å, below the detection limit of nitrogen, which extends up to 13 Å. At 800 ºC, when the time is extended to 12 hours, a very intense peak centred at 7 Å is observed, the pores being wider than at 6 hours. When the temperature is increased to 900

°C or 950 ºC, narrow micropores centred at 8 Å is observed, but also the presence of porosity that extends to sizes up to 20 Å. The sample prepared using the oxidized PU, PUox800 6H, presents wider pores than the homologous without oxidation, which extends to the mesopores range.

Data in Table 2 also reveals the importance of narrow pore size distribution for the CO_2 adsorption process at 25ºC, where an intense adsorption potential is needed for the interactions to be strong enough to adsorb CO_2. In this case, PU 950 7H reduces drastically the CO_2 adsorption capacity at 25ºC, whereas PU 800 6H maintain almost the same values at 0 and 25ºC, hence indicating the presence of very narrow porosity, which is fully contributing to adsorption at both temperatures. On the other hand, in PUox 800 6H sample the adsorption capacity at 25ºC is reduced, which indicates that very narrow porosity is present in the sample, but not as narrow as in the homologous PU 800 6H sample.

Table 2. Comparison of the CO_2 adsorption (N_{CO2}) s at 0 °C and 25ºC.

Sample	**N_{CO2} at 0ºC (mmol/g)**	**N_{CO2} at 25ºC (mmol/g)**
PUox 800 6H	3.7	3.0
PU 800 6H	1.5	1.4
PU 900 6H	2.8	2.5
PU 800 12H	2.5	2.2
PU 950 7H	3.4	1.9

Figure 3 shows the kinetic profiles obtained for the samples. The PU-derived carbons (PU and PUox) activated at 800ºC during 6 h present the lowest methane adsorption values, which suggests that there is no methane adsorption, since they adsorb between 0.01 and 0.02 mmol/g, which fits within the experimental error. Moreover, the PU 800 6H sample does not adsorb nitrogen and hence it is not possible to adsorb methane.

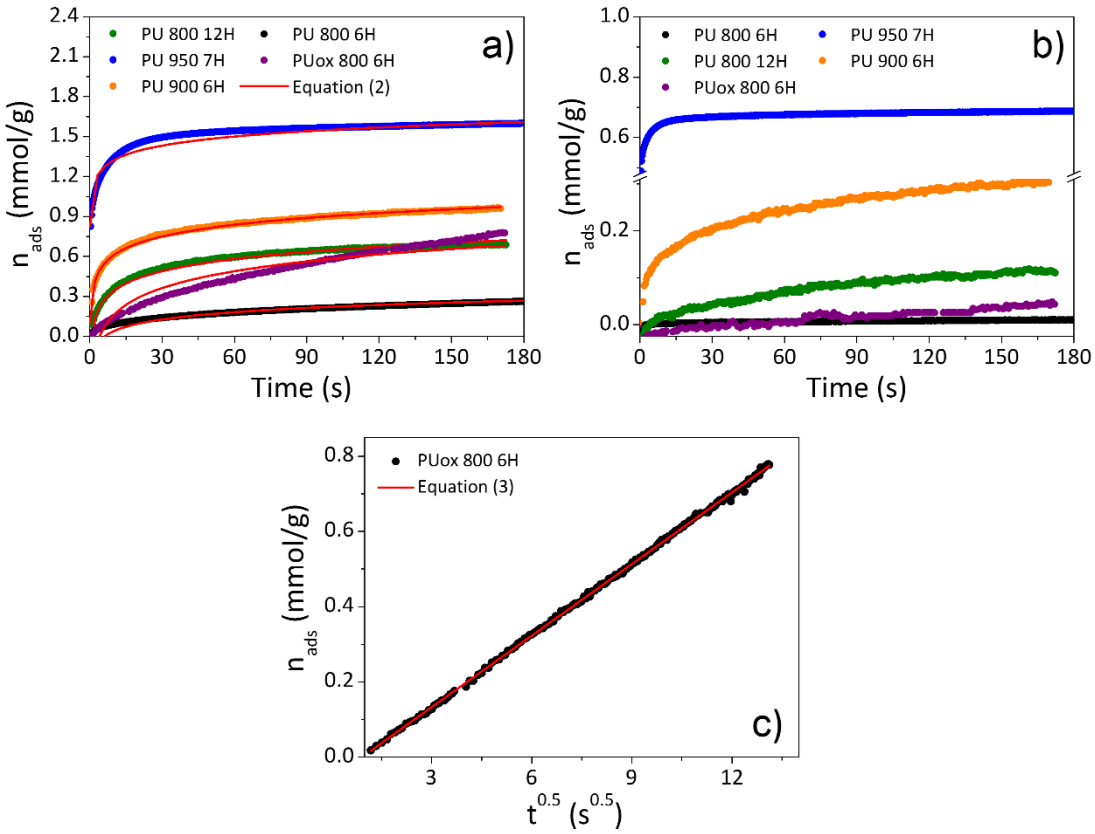

Figure 3. Kinetic experiment profiles performed; (a) CO_2 adsorption; (b) CH_4 adsorption; (c) CO_2 adsorption in function of $t^{0.5}$. Red lines are fittings to the obtained kinetic profiles of CO_2 adsorption.

The shape of the CO_2 adsorption profiles can be fitted into a logarithmic equation almost perfectly, similar to a type I nitrogen isotherm, which corresponds to the Elovich kinetic model, except for the case of PUox 800 6H sample, in which the adsorbed amount is linearly dependent on $t^{0.5}$ (Fig. 3c), typically found for adsorption dominated by intraparticle diffusion model [17].

Kinetic models allow the identification of the rate controlling processes occurring during the adsorption. The rate controlling process, also called limiting process, is the slowest process taking place, and hence, is the one with most impact in the kinetics. There are several mechanisms occurring, which are related with physical and/or chemical interactions that can be identify by fitting the profiles obtained with the equation that govern

each mechanism. The main important mechanism occurring are adsorption/chemisorption processes, and diffusion related ones such as intraparticle diffusion [17].

Elovich model is usually applied to heterogeneous samples undergoing chemisorption processes [18], and it is governed by the Equation (1).

$$\frac{dn_t}{dt} = ae^{(-bn_t)} \qquad (1)$$

Where a and b are constants, and after the integration assuming that initially n_0=0 and t_0=0, becomes Equation (2) and hence, the plot of the amount adsorbed versus ln(t) must follow a linear plot.

$$n_t = \frac{1}{b}\ln(ab) + \frac{1}{b}\ln(t) \;\; ; \;\; n_t = C + A ln(t) \qquad (2)$$

All the adsorption profiles except those activated at 800 °C show a good correlation with this process, which indicates that adsorption is the rate controlling process, and hence, the slowest. This evidence is in good agreement with the textural characterization, since pore size is wider and therefore the adsorption is less favoured. On the other hand, the shape of the adsorption data of PU 800 6H indicates that there are some intervals where adsorption is actually the dominant feature. Regarding PUox 800 6H, adsorption is clearly not the rate controlling step of the process. Therefore, in order to asset that diffusion is the limiting mechanism, the intraparticle diffusion model was evaluated. Intraparticle diffusion model is governed by equation (3), where K represents the intraparticle diffusion constant, and C represents the boundary layer thickness, defined as the length of the solute material perpendicular to the adsorbent whose velocity is 0.99 times of the flow. It predicts that once a process is mainly dominated by diffusion steps, the plot of the amount adsorbed at a certain time *versus* $t^{0.5}$ must follow a linear progression that crosses the origin [19]. Deviation from the origin would meant that there are other processes occurring along with the diffusion.

$$n_t = C + K\sqrt{t} \qquad (3)$$

Equation (3) fits well to sample Puox 800 6H profile (R^2=0.9996), once representing the amount adsorbed versus $t^{0.5}$. However, the boundary layer thickness I is negative, which could be related with the adsorption processes taking place, where negative values could mean that the solute is actually crossing within the adsorbent.

Figure 4 shows the fit of different stages for PU 800 6H activated carbons. There are two distinct regions in the process: i) where adsorption governs the system and hence the system is in concomitance with Elovich model, which is applicable in the first 5 seconds, with high correlation, and ii) where intraparticle diffusion is the main process, which usually occurs in activated carbons [17,20]. There is also a transition region between 5-20 seconds, where both, adsorption and intraparticle diffusion concomitant occur.

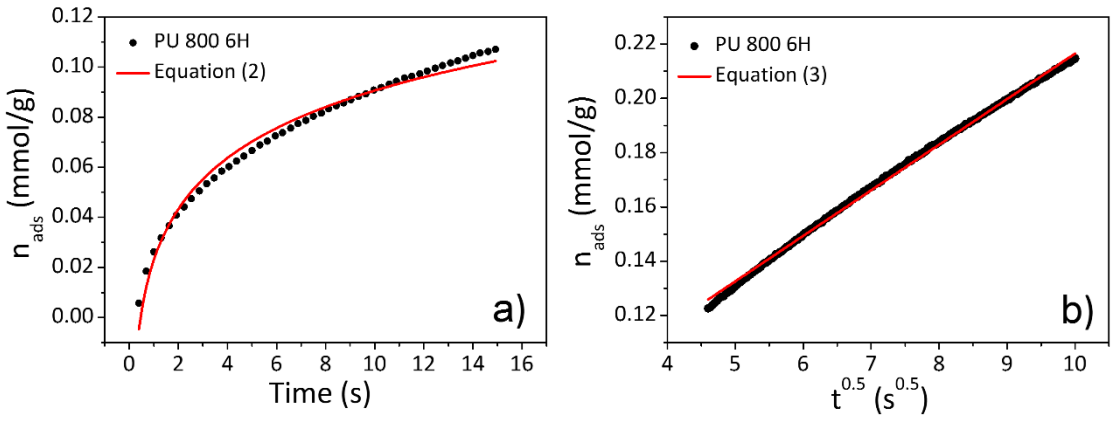

Figure 4. Fitting curves of PU 800 6H kinetic adsorption applying: (a) Elovich model and (b) Intraparticle diffusion model.

Table 3 shows a comparison of the selectivity obtained including a typical commercial molecular sieve (Zeolite 4A). All the samples adsorb CO_2 preferably than methane, but the mentioned samples PUox 800 6H and PU 800 6H exhibit a substantially high selectivity for CO_2, since they adsorb very small amounts of methane and therefore, these samples are extremely interesting from an industrial point of view. The PUox-derived carbon adsorbs almost 32 times more CO_2 after 120 s, and the PU 800 6H sample 23 times

more. Nevertheless, the amount adsorbed by all PU-derived carbons after 120 s is lower than the zeolite. The lower interactions of these materials with CO_2 should lead to an easier regeneration during separation processes [21,22].

Table 3. Comparison of the selectivity and adsorption values for the materials obtained and reference material.

Sample	n_{CO2} at 120 s (mmol/g)	n_{CH4} at 120 s (mmol/g)	n_{CO2}/n_{CH4}
Zeolite 4A	2.89	0.14	21
PU 800 6H	0.23	0.01	23
PUox 800 6H	0.64	0.02	32
PU 800 12H	0.67	0.10	7
PU 900 6H	0.92	0.29	3
PU 950 7H	1.58	0.67	2

The results suggest that PUox 800 6H and PU 800 6H carbons should be efficient, with almost total selectivity of CO_2 *versus* methane in a typical PSA process, despite the absence of pressure. Since these samples do not adsorb any methane after 60 s, and intraparticle diffusion is the limiting process in CO_2 adsorption, an increase in pressure will favour this feature, due to the increasing of diffusivity at higher pressures. Moreover, the results indicate that both samples activated at 800 ºC have a very high affinity for CO_2, being interesting materials for CO_2/CH_4 separation. Their adsorption behaviour is mainly determined by diffusion, however, they present several differences that must be discussed. PUox 800 6H is fully governed by diffusion, even at the beginning of the kinetic experiment, and hence, has more affinity for CO_2. The wider porosity of this sample should also enhance the diffusion processes within the pores. However, its adsorption behaviour indicates that there is a high CO_2 affinity, as well as a low diffusion rate, caused by strong interactions, which inhibit CO_2 to diffuse.

Since heteroatoms such as nitrogen and oxygen could have influence in the adsorption interactions, and PUox sample underwent a previous oxidizing treatment, XPS analysis were performed. **Figure 5** shows the XPS spectra of the AC's. In the spectra of Fig. 5a (O1s) the peak located between 531.4–531.8 eV corresponds to the C=O double bound in carbonyl and lactones. The peak centred between 532 – 533 eV is assigned to C-O single bond in aromatic rings, ethers and phenols, and the peak at between 533 – 535 eV is related with water and chemisorbed oxygen. In the spectra of Fig. 5b (N1s), peaks corresponding to pyridinic (398.5 – 398.2 eV), pyrrolic, (400.5 – 400.9 eV) and quaternary (403.1 eV) nitrogen functionalities are displayed, respectively.

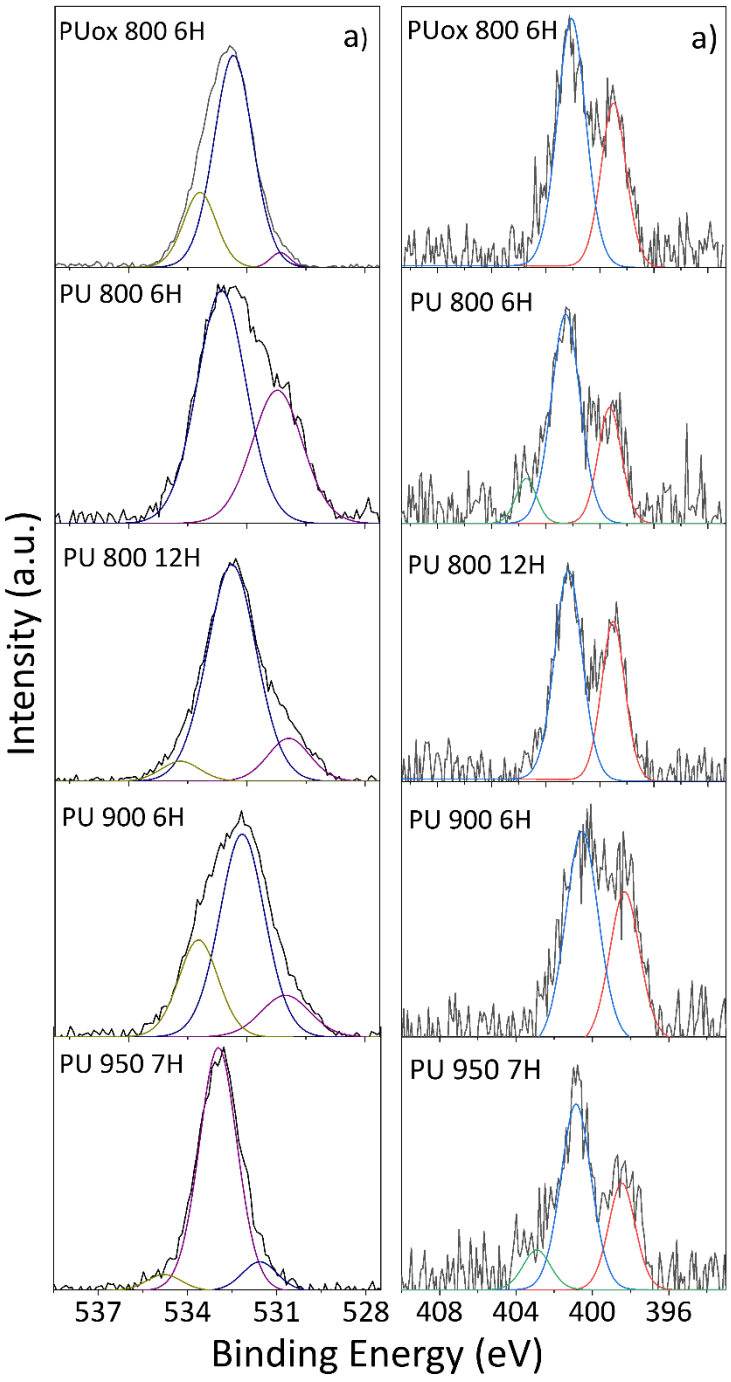

Figure 5. XPS spectra of the AC's: (a) O1s orbitals (b) N1s orbitals.

Surface atomic percent of nitrogen and oxygen functionalities are shown in **Table 4** and **Table 5**, respectively. There are very small differences in the amounts of nitrogen, and the main N functionalities are pyrrolic and pyridinic, whereas some quaternary nitrogen species can also be found. These small variations alone do not explain the amounts of CO_2

adsorbed, since there are notable differences of adsorption related with porosity and all the samples have approximately the same nitrogen amounts and functionalities.

Table 4. Atomic percent of Nitrogen functionalities calculated from N1s orbital.

	N_{1s} (at.%)			
Sample	$N_{pyrrolic}$	$N_{pyridinic}$	$N_{quaternary}$	N_{total}
PU 800 6H	0.5	1.2	0.2	1.9
PUox 800 6H	0.8	1.3	0	2.1
PU 800 12H	1.2	1.8	0	3.0
PU 900 6H	0.9	1.3	0	2.2
PU 950 7H	0.7	1.3	0.3	2.3

Oxygen functionalities (Table 5) of C-O-R and acidic species are present in most samples [23-25]. However, the C=O groups is present only in the sample PU 950 7H. The ones found at 530.7eV correspond to contamination of alumina, probably from the crucible used for the activation of the samples. The evolution of oxygen species and the differentiation of the types of oxygen with XPS is a difficult task mainly due to the variety of different functional groups able to be formed [26]. However, there is an important difference in the amount of O groups between PUox 800 6H and PU 800 6H AC's, which is caused by the forced oxidative process applied (PUox), which led to a higher oxygen content in this sample.

Table 5. Atomic percent of Oxygen functionalities calculated from O1s orbital.

	O_{1s} (at.%)					
Sample	$O^{530.7eV}$	$O^{531.6eV}$	$O^{532.3eV}$	$O^{533.6eV}$	$O^{534.4eV}$	O^{total}
PU 800 6H	0	0	3.1	1.6	0	4.7
PUox 800 6H	0.3	0	8.7	2.6	0	10.4
PU 800 12H	1.5	0	9.0	0	0.7	11.2
PU 900 6H	1.4	0	6.4	2.7	0	10.5
PU 950 7H	0	0.7	5.8	0	0.4	6.8

It is possible that surface chemistry presents certain influence in the kinetic experiments performed. It has been studied in previous works that O functionalities have a negative influence in methane adsorption [27]. However, the effect of oxygen functionalities regarding CO_2 adsorption is not completely clear, although the presence of basic O groups such as pyrones could enhance CO_2 adsorption due to the acidic character of CO_2 [28]. Some studies actually claim that the increase of surface groups enhances the adsorption efficiency [29]. In this case, the increase of oxygen groups leads to processes governed by diffusion instead of adsorption, which is the case of PUox 800 6H AC's when compared to the non-pre-treated PU 800 6H.

4. Conclusion

PU foam residues are suitable materials for the preparation of activated carbon molecular sieves. The activation with CO_2 leads to highly microporous materials with extremely small pore size, which, in some cases, avoids the adsorption of nitrogen at -196ºC. The small pore size was confirmed with nitrogen and CO_2 isotherms, since most of the samples present higher pore volume available for CO_2. Kinetic of adsorption measurements were performed to asset the selectivity and behaviour of the samples and evaluate their use as molecular sieves for the separation of CO_2/CH_4 mixtures. The kinetic studies confirmed that samples have high selectivity towards CO_2 adsorption, being able to adsorb up to 32 times more CO_2 than methane after 180 seconds. The kinetic behaviour of the samples activated at 800ºC during 6 h was different than in the other samples, which followed the Elovich model of adsorption, where the adsorption process is the limiting step; therefore, the adsorption is less efficient in these samples. Moreover, in these samples, intraparticle diffusion is the slowest process, favouring CO_2 adsorption. Nevertheless, these samples have textural and kinetic differences. The adsorption kinetics of the pre-oxidized sample is fully governed by

diffusion, whereas for the non-oxidized sample, in the first 15 s adsorption is the limiting step. The differences arise from the increase of surface groups and pore size in PUox 800 6H, which provided evidence that certain oxygen groups are able to interact with CO_2 enabling its adsorption, and at the same time increasing repulsion against CH_4, being this sample with both, higher selectivity and higher CO_2 adsorption.

Acknowledgements

This research was funded by MINECO (MAT2016-80285-p), GV (PROMETEOII/2014/004), H2020 (MSCA-RISE-2016/NanoMed Project). Financial support of the National Council for Scientific and Technological Development (CNPq-Brazil) is also acknowledged.

Declaration of competing interest

The authors declare no conflicts of interest.

CRediT authorship contribution statement

Orlando F. Cruz Jr.: Conceptualization, InvestigationWriting- Original draft preparation, Methodology. **Ignacio Campello Gómez:** Conceptualization, Investigation, Methodology, Writing - Review & Editing. **Manuel Martinez Escandell1:** Funding acquisition, Supervision, Writing - Review & Editing. **Carlos R. Rambo:** Validation, Visualization, Writing- Reviewing and Editing. **Joaquín Silvestre-Albero:** Writing - Review & Editing,Funding acquisition, Project administration.

References

[1] A. Stips, D. MacIas, C. Coughlan, E. Garcia-Gorriz, X.S. Liang, Sci. Reports 2016

61 (2016) 1–9. https://doi.org/10.1038/srep21691.

[2] A. Petersson, A. Wellinger, Biogas upgrading technologies – developments and innovations, IEA Bioenergy, 2009.

[3] N. Cui, Biomethane as Transport Fuel Potential in Finland, BS Thesis, Finland, 2015.

[4] E. Ryckebosch, M. Drouillon, H. Vervaeren, Biomass and Bioenergy. 35 (2011) 1633–1645. https://doi.org/10.1016/J.BIOMBIOE.2011.02.033.

[5] Q. Zhao, E. Leonhardt, C. MacConnell, C. Frear, S. Chen, Clim. Friendly Farming Improv. Carbon Footpr. Agric. Pacific Northwest. CSANR Res. Rep. 2010-00. (2010) 24.

[6] E.E. Ünveren, B.Ö. Monkul, Ş. Sarıoğlan, N. Karademir, E. Alper, Petroleum 3 (2017) 37–50. https://doi.org/10.1016/j.petlm.2016.11.001.

[7] M.J. Tuinier, M. van Sint Annaland, Ind. Eng. Chem. Res. 51 (2012) 5552–5558. https://doi.org/10.1021/ie202606g.

[8] M. Tagliabue, D. Farrusseng, S. Valencia, S. Aguado, U. Ravon, C. Rizzo, A. Corma, C. Mirodatos, Chem. Eng. J. 155 (2009) 553–566. https://doi.org/10.1016/J.CEJ.2009.09.010.

[9] P. Riemer, I. Webster, W. Ormerod, H. Audus, Fuel 73 (1994) 1151–1158. https://doi.org/10.1016/0016-2361(94)90252-6.

[10] J. Serafin, M. Ouzzine, O.F. Cruz, J. Sreńscek-Nazzal, I. Campello Gómez, F.-Z. Azar, C.A. Rey Mafull, D. Hotza, C.R. Rambo, Waste Manag. 136 (2021) 273–282. https://doi.org/10.1016/j.wasman.2021.10.025

[11] O. F. Cruz, J. Silvestre-Albero, M.E. Casco, D. Hotza, C.R. Rambo, Mater. Chem. Phys. 216 (2018) 42-46. https://doi.org/10.1016/j.matchemphys.2018.05.079.

[12] F. Yang, W. Li, R. Ou, Y. Lu, X. Dong, W. Tu, W. Zhu, X. Wang, L. Li, A. Yuan, J. Pan, Chinese Journal of Chemical Engineering 47 (2022) 120-133. https://doi.org/10.1016/j.cjche.2021.02.013.

[13] F. Yang, W. Li, X. Zhong, W. Tu, J. Cheng, L. Chen, J. Lu, A. Yuan, J. Pan, Separation and Purification Technology 297 (2022) 121415. https://doi.org/10.1016/j.seppur.2022.121415.

[14] W. Li, W. Tu, J. Cheng, F. Yang, X. Wang, L. Li, D. Shang, X. Zhou, C.Yu, A. Yuan, J. Pan, Separation and Purification Technology 282 Part A (2022) 120001. https://doi.org/10.1016/j.seppur.2021.120001.

[15] PlasticsEurope, Plastics – the Facts 2010, Plast. – Facts 2010. (2010) www.plasticseurope.de/informations.

[16] M.M.M. Dubinin, Carbon 27 (1989) 457–467. https://doi.org/10.1016/0008-6223(89)90078-X.

[17] B. Li, Q. Zhang, C. Ma, IOP Conf. Ser. Earth Environ. Sci. 121 (2018). https://doi.org/10.1088/1755-1315/121/2/022019.

[18] G. William Kajjumba, S. Emik, A. Öngen, H. Kurtulus Özcan, S. Aydın, Modelling of Adsorption Kinetic Processes—Errors, Theory and Application, in: Adv. Sorption Process Appl., IntechOpen, 2019. https://doi.org/10.5772/intechopen.80495.

[19] G. Varank, A. Demir, K. Yetilmezsoy, S. Top, E. Sekman, M.S. Bilgili, Indian J. Chem.Techn. 19 (2012) 7-25.

[20] N. Álvarez-Gutiérrez, M.V. Gil, F. Rubiera, C. Pevida, Chem. Eng. J. 307 (2017) 249–257. https://doi.org/10.1016/j.cej.2016.08.077.

[21] M. Antonio-Abdu Sami, V. Eliseo, MATEC Web Conf. 192 (2018) 03029. https://doi.org/10.1051/matecconf/201819203029.

[22] L. Hauchhum, P. Mahanta, Int. J. Energy Environ. Eng. 5 (2014) 349–356. https://doi.org/10.1007/s40095-014-0131-3.

[23] S. Delpeux, F. Beguin, R. Benoit, R. Erre, N. Manolova, I. Rashkov, FEur. Polym. J. 34 (1998) 905–915. https://doi.org/10.1016/S0014-3057(97)00225-5.

[24] S.D. Gardner, C.S.K. Singamsetty, G.L. Booth, G.R. He, C.U. Pittman, Carbon 33 (1995) 587–595. https://doi.org/10.1016/0008-6223(94)00144-O.

[25] L.T. Weng, C. Poleunis, P. Bertrand, V. Carlier, M. Sclavons, P. Franquinet, R. Legras, J. Adhes. Sci. Technol. 9 (1995) 859–871. https://doi.org/10.1163/156856195X00743.

[26] J.. L. Figueiredo, M.F.. F.R. Pereira, M.M.. M.A. Freitas, J.J.. J.M. Órfão, Carbon 37 (1999) 1379–1389. https://doi.org/10.1016/S0008-6223(98)00333-9.

[27] S. Hao, J. Wen, X. Yu, W. Chu, Appl. Surf. Sci. 264 (2013) 433–442. https://doi.org/10.1016/j.apsusc.2012.10.040.

[28] D. Saha, M.J. Kienbaum, Microporous Mesoporous Mater. 287 (2019) 29–55. https://doi.org/10.1016/j.micromeso.2019.05.051.

[29] Y.-C. Chiang, C.-Y. Yeh, C.-H. Weng, Appl. Sci. 9 (2019) 1977. https://doi.org/10.3390/app9101977.